

Quantum-dot lithium in zero magnetic field: Electronic properties, thermodynamics, and a liquid-solid transition in the ground state

S. A. Mikhailov*

Theoretical Physics II, Institute for Physics, University of Augsburg, 86135 Augsburg, Germany

(December 2, 2024)

Energy spectra, electron densities, pair correlation functions and heat capacity of a quantum-dot lithium in zero external magnetic field (a system of three interacting two-dimensional electrons in a parabolic confinement potential) are studied using the exact diagonalization approach. A particular attention is given to a Fermi-liquid – Wigner-solid transition in the ground state of the dot, induced by the intra-dot Coulomb interaction.

PACS numbers: 73.21.La, 73.20.Qt, 71.10.-w

I. INTRODUCTION

Quantum dots¹ are artificial electron systems (ES) realizable in modern semiconductor structures. In these systems two-dimensional (2D) electrons move in the plane $z = 0$ in a lateral confinement potential $V(x, y)$. The typical length scale l_0 of the lateral confinement is usually larger than or comparable with the effective Bohr radius a_B of the host semiconductor. The relative strength of the electron-electron and electron-confinement interaction, given by the ratio $\lambda \equiv l_0/a_B$, can be varied, even experimentally, in a wide range, so that the dots are used to be treated as artificial atoms with tunable physical properties. Experimentally, quantum dots were intensively studied in recent years, using a variety of different techniques, including capacitance², transport³, far-infrared⁴ and Raman spectroscopy⁵.

From the theoretical point of view, quantum dots are ideal physical objects for studying effects of electron-electron correlations. Different theoretical approaches, including analytical calculations^{6–10}, exact diagonalization^{11–25}, quantum Monte Carlo (QMC)^{26–34}, density functional theory^{35–39} and other methods^{40–45}, were applied to study their properties. Until recently most theoretical work was performed in the regime of strong magnetic fields, when all electron spins are fully polarized. In the past three years a growing interest is observed in studying the quantum dot properties in zero magnetic field $B = 0$ ^{23,24,31,32,34,44,45}. The aim of these studies is to investigate the Fermi liquid – Wigner cluster crossover in the dots, at a varying strength of Coulomb interaction. Detailed knowledge of the physics of such a crossover in microscopic dots could be compared with that obtained for macroscopic 2DES^{46,47} and might shed light on the nature of the metal-insulator transition in two dimensions⁴⁸.

So far, full energy spectra of an N -electron parabolic quantum dot in zero magnetic field, as a function of the interaction parameter λ , were published only for $N = 2$ ¹² (quantum-dot helium). For larger N a number of results for the ground state energy of the dots were reported at separate points of the λ axis. Sometimes, however, results obtained by different methods contradict to each other, and full understanding of physical properties of N -electron dots at $B = 0$ has not yet been achieved.

Even for three electrons in a parabolic confining potential (quantum-dot lithium) available in the literature results are somewhat confusing and do not give a clear and exact picture of the ground state of the dot. Egger et al. reported in³¹ on a transition from a partly to a fully spin-polarized ground state at $\lambda \approx 5$ caused by the intra-dot Coulomb interaction (z -component of the total spin S_z^{tot} changes from $1/2$ to $3/2$). This conclusion was based on results of QMC calculations (multilevel blocking algorithm). For the $1/2$ state calculations gave *slightly lower* energy, than for the $3/2$ state, at $\lambda = 4$, and higher energies at $\lambda = 6, 8$ and 10 . In a subsequent (Erratum) publication³² other (corrected) values for the energy of these states were reported. At $\lambda = 4$ they gave *the same* energies of the $1/2$ and $3/2$ states. The conclusion from these two publications in the part concerning the three-electron quantum dot is thus not clear. Häusler⁴⁴, calculating the energy spectrum of a three-electron dot using the so-called pocket state method, gave a more definite indication on the existence of such a transition. He presented his results, however, in some specific for the method and not-directly related to λ units, which does not allow one to quantitatively characterize the transition (e.g. to get the value of the interaction parameter λ at the transition point). Häusler also pointed out that some indications on such a transition can be also seen in earlier studies of a three-electron dot: in Ref.¹⁵ ($\lambda \approx 2$) the ground state of the dot at $B = 0$ was found to be partly spin-polarized, while in Ref.⁴¹ with a substantially larger value of λ the fully spin-polarized state turned out to have the lower energy. As seen from this brief outline, available data indicate that this transition seems to exist but it is not yet quantitatively understood, and its physical origin is not completely clear. It is also not clear whether or not this transition in the spin state of the system is related to the Fermi-liquid – Wigner molecule transition in the dot.

In this paper I present results of a complete theoretical study of a three-electron parabolic quantum dot. Using exact diagonalization technique, I calculate full energy

spectrum of the dot, as a function of the interaction parameter in the range $0 \leq \lambda \leq 10$. At $\lambda = \lambda_c = 4.343$ I find a transition in the ground state of the dot, accompanied by the change of the *total spin* quantum number (not the projection of the total spin). I study the densities and the pair-correlation functions in the ground and the first excited states of the system at a number of λ -points, including the vicinity of the transition. These results show that physical properties of the dot dramatically change at the transition point, so that it can be treated as a liquid-solid transition. I also calculate some thermodynamic properties of the dot: the heat capacity and the volume-pressure diagram. The temperature dependence of the heat capacity clearly exhibits characteristic features, related to the transition, in the temperature range corresponding to a few K for typical parameters of GaAs dots. Other experimental consequences from predictions of this paper are also discussed.

In Section II I briefly describe the model and the method used in calculations. Results of the work are presented in Section III. Discussions and conclusions can be found in Section IV.

II. MODEL AND METHOD

A. The Hamiltonian

I consider three 2D electrons moving in the plane $z = 0$ in a parabolic confining potential $V(r) = m^* \omega_0^2 r^2 / 2$, $\mathbf{r} = (x, y)$. The Hamiltonian of the system

$$\hat{H} = \sum_{i=1}^N \left(\frac{\hat{\mathbf{p}}_i^2}{2m^*} + \frac{m^* \omega_0^2 \mathbf{r}_i^2}{2} \right) + \frac{1}{2} \sum_{i \neq j=1}^N \frac{e^2}{|\mathbf{r}_i - \mathbf{r}_j|} \quad (1)$$

($N = 3$) commutes with operators of the total angular momentum \hat{L}_z^{tot} , (squared) total spin $\hat{\mathbf{S}}_{tot}^2$ and projection of the total spin \hat{S}_ζ^{tot} on some (ζ -) axis (not necessarily coinciding with the z -axis). This gives three conserving quantum numbers $L_{tot} \equiv L_z^{tot}$, S_{tot} and S_ζ^{tot} . No magnetic field is assumed to be applied to the system.

B. Basis set of single-particle states

A complete set of single-particle solutions of the problem

$$\phi_{nls}(\mathbf{r}, \sigma) = \varphi_{nl}(\mathbf{r}) \chi_s(\sigma) \quad (2)$$

is a product of the Fock-Darwin orbitals^{49,50}

$$\varphi_{nl}(\mathbf{r}) = \frac{1}{l_0} \sqrt{\frac{n!}{\pi(n+|l|)!}} \left(\frac{r}{l_0} \right)^{|l|} e^{i l \theta - r^2 / 2l_0^2} L_n^{|l|}(r^2 / l_0^2) \quad (3)$$

and the spin functions $\chi_s(\sigma)$. Here

$$l_0 = \sqrt{\hbar / m^* \omega_0} \quad (4)$$

is the oscillator length, and (n, l, s) are the radial, azimuthal (angular momentum) and spin quantum numbers of the single-particle problem ($n \geq 0$ and l are integer, $s = \pm 1/2$). All the single-particle states (2) can be ordered and enumerated, e.g. $\phi_1 \equiv (nls)_1 = (0, 0, \uparrow)$, $\phi_2 = (0, 0, \downarrow)$, $\phi_3 = (0, 1, \uparrow)$, etc. The energy of the states (2) does not depend on spins,

$$E_{nls} = \hbar \omega_0 (2n + |l| + 1). \quad (5)$$

C. Basis set of many-particle states

A complete set of many-particle states Ψ_u , $u = 1, 2, \dots$ is formed by placing particles in different single-particle states, e.g.

$$\Psi_1 = |\phi_1 \phi_2 \phi_3\rangle, \Psi_2 = |\phi_1 \phi_2 \phi_4\rangle, \Psi_3 = |\phi_1 \phi_5 \phi_8\rangle, \dots \quad (6)$$

where $|\phi_\alpha \phi_\beta \phi_\gamma\rangle$ are Slater determinants

$$|\phi_\alpha \phi_\beta \phi_\gamma\rangle = \frac{1}{\sqrt{3!}} \det \begin{vmatrix} \phi_\alpha(\xi_1) & \phi_\beta(\xi_1) & \phi_\gamma(\xi_1) \\ \phi_\alpha(\xi_2) & \phi_\beta(\xi_2) & \phi_\gamma(\xi_2) \\ \phi_\alpha(\xi_3) & \phi_\beta(\xi_3) & \phi_\gamma(\xi_3) \end{vmatrix} \quad (7)$$

and $\xi_i = (\mathbf{r}_i, \sigma_i)$. All the many-particle states Ψ_u can be also arranged, e.g. in order of increasing of their total single-particle energy

$$E_u^{sp} = E_{(nls)_\alpha} + E_{(nls)_\beta} + E_{(nls)_\gamma}, \quad (8)$$

and enumerated.

D. Solution of the Schrödinger equation

Expanding the many-body wave function in a complete set of many-particle states,

$$\Psi(\xi_1, \xi_2, \xi_3) = \sum_u C_u \Psi_u(\xi_1, \xi_2, \xi_3), \quad (9)$$

I get the Schrödinger equation in the matrix form,

$$\sum_{u'} (H_{uu'} - E \delta_{uu'}) C_{u'} = 0. \quad (10)$$

The conservation of the total angular momentum L_{tot} and the projection of the total spin S_ζ^{tot} allows one to choose the many-body states for the expansion (9) under additional constraints

$$\sum_{i=1}^N l_i = L_{tot}, \quad \sum_{i=1}^N s_i = S_\zeta^{tot}. \quad (11)$$

This reduces the size of the matrix in (10) and facilitates calculations.

Numerically diagonalizing the eigenvalue problem (10) I get a set of energy levels

$$E_{L_{tot}, S_{\zeta}^{tot}, m} = \hbar\omega_0 \mathcal{F}_{L_{tot}, S_{\zeta}^{tot}, m}(\lambda), \quad (12)$$

and corresponding eigenfunctions

$$\Psi_{L_{tot}, S_{\zeta}^{tot}, m} = \sum_u C_u^{L_{tot}, S_{\zeta}^{tot}, m}(\lambda) \Psi_u, \quad (13)$$

as a function of the interaction parameter $\lambda = l_0/a_B$. The number $m = 1, 2, \dots$ enumerates the energy levels of the system in the subspace of levels with given L_{tot} and S_{ζ}^{tot} . After the diagonalization problem is solved, the eigenvalues of the total spin are calculated for each level m from

$$S_{tot}(S_{tot} + 1) = \langle \Psi_{L_{tot}, S_{\zeta}^{tot}, m} | \hat{S}_{tot}^2 | \Psi_{L_{tot}, S_{\zeta}^{tot}, m} \rangle. \quad (14)$$

All the matrix elements of the Hamiltonian $H_{uu'}$ and of the operator $(\hat{S}_{tot}^2)_{uu'}$ are calculated analytically.

All the energy levels with non-zero L_{tot} and S_{ζ}^{tot} are degenerate,

$$E_{L_{tot}, S_{\zeta}^{tot}} = E_{-L_{tot}, S_{\zeta}^{tot}} = E_{L_{tot}, -S_{\zeta}^{tot}} = E_{-L_{tot}, -S_{\zeta}^{tot}}. \quad (15)$$

Presenting below results for the energy of the states $(L_{tot}, S_{\zeta}^{tot})$, I omit the corresponding signs [for instance, $(1, 1/2)$ stands for $(\pm 1, \pm 1/2)$ with all possible combinations of signs]. Degeneracy of levels are calculated accounting for (15).

E. Properties of the states and the heat capacity

After the Schrödinger problem is solved and all the energy levels and the eigenfunctions are found, I calculate the density of spin-up and spin-down polarized electrons in the states $(L_{tot}, S_{\zeta}^{tot}, m)$, and the corresponding pair-correlation functions. These quantities are calculated as averages of the operators

$$\hat{n}_{\sigma}(\mathbf{r}) = \sum_{i=1}^N \delta(\mathbf{r} - \mathbf{r}_i) \delta_{\sigma\sigma_i} \quad (16)$$

and

$$\hat{P}_{\sigma\sigma'}(\mathbf{r}, \mathbf{r}') = \sum_{i=1}^N \sum_{j=1, \neq i}^N \delta(\mathbf{r} - \mathbf{r}_i) \delta(\mathbf{r}' - \mathbf{r}_j) \delta_{\sigma\sigma_i} \delta_{\sigma'\sigma_j} \quad (17)$$

with the eigenfunctions $\Psi_{L_{tot}, S_{\zeta}^{tot}, m}$. All the matrix elements of the operators (16) and (17) are calculated analytically.

As the method offers an opportunity to find all the energy levels of the system, one can also calculate thermodynamic properties of the dots. I calculate the heat capacity as $C_{\lambda} = (\partial \bar{E} / \partial T)_{\lambda}$, where

$$\bar{E} \equiv \bar{E}(\lambda, T) = \frac{\sum_n E_n(\lambda) e^{-E_n(\lambda)/T}}{\sum_n e^{-E_n(\lambda)/T}}, \quad (18)$$

T is the temperature, and the sum is taken over all (low-lying) energy levels accounting for their degeneracies.

F. Convergency of the method

The number of all many-particle states in the problem is infinite, and the size of the matrix $H_{uu'}$ in Eq. (10) is infinite too. To perform practical calculations I restrict the number of many-particle states in the expansion (9) so that the total single-particle energy (8) of the involved many-body states is smaller than some threshold value E_{th} , $E_u^{sp} \leq E_{th}$. The larger the threshold energy E_{th} , the broader the range of λ in which results are convergent and reliable. Typically, less than 1000 many-particle states were sufficient for all the calculations presented below.

Convergency of the method is illustrated on Figure 1, where the energy of the lowest state ($m = 1$) with $(L_{tot}, S_{tot}) = (1, 1/2)$ is shown as a function of $\lambda = l_0/a_B$ for increasing threshold energy E_{th} . The curves are labeled by the number of many-body quantum states involved in the expansion (9). One sees that including about 1000 many-body states leads to very accurate results for the energy at $\lambda \leq 20$. Notice that below I present results for the energy in the interval $\lambda \leq 10$, where the method is practically exact.

III. RESULTS

All the lengths in this Section are measured in units l_0 , all the energies – in units $\hbar\omega_0$, the densities and the pair-correlation functions – in units $(\pi l_0^2)^{-1}$ and $(\pi l_0^2)^{-2}$ respectively.

A. Preliminary notes

The interaction parameter in the problem

$$\lambda = \frac{l_0}{a_B} \propto \frac{e^2}{\hbar^{3/2}} \quad (19)$$

characterizes the relative strength of classical Coulomb ($\sim e^2$) and quantization effects ($\sim \hbar$). The limit of small λ corresponds to a weakly interacting system ($e^2 \rightarrow 0$) and can be treated exactly. The ground state in this limit is realized in the configuration $[(0, 0, \uparrow)(0, 0, \downarrow)(0, 1, \uparrow)]$, i.e. $(L_{tot}, S_{tot}) = (1, 1/2)$, with the energy

$$\lim_{\lambda \rightarrow 0} \frac{E_{GS}}{\hbar\omega_0} = 4. \quad (20)$$

The opposite case $\lambda \rightarrow \infty$ corresponds to the purely classical limit ($\hbar \rightarrow 0$). In the classical ground state, electrons occupy the corners of an equilateral triangle^{51,52}, with the distance

$$R_{cl} = l_{cl}/3^{1/6} \quad (21)$$

from the origin, and the ground state energy is

$$E_{GS}^{cl} = \frac{3^{5/3}}{2} \epsilon_{cl} = \frac{3^{5/3}}{2} \frac{e^2}{l_{cl}}. \quad (22)$$

Here l_{cl} and ϵ_{cl} are the classical length and energy units,

$$l_{cl} = \left(\frac{e^2}{m^* \omega_0^2} \right)^{1/3} = \left(\frac{l_0^4}{a_B} \right)^{1/3}, \quad \epsilon_{cl} = \frac{e^2}{l_{cl}}. \quad (23)$$

So, in the classical limit

$$\lim_{\lambda \rightarrow \infty} \frac{E_{GS}}{\hbar\omega_0} = \frac{3^{5/3}}{2} \lambda^{2/3}. \quad (24)$$

Results for the energy of the ground and excited states at arbitrary λ are presented in the next Section.

B. Energy spectra

1. Exact results

Figure 2 shows the low-lying energy levels of a three-electron parabolic quantum dot with the total angular momentum $L_{tot} = 1$. Shown are only the states which start from $E/\hbar\omega_0 \leq 6$ at $\lambda = 0$. The lowest-energy state (the ground state in the subspace of levels with $L_{tot} = 1$) corresponds (in the limit $\lambda \rightarrow 0$) to the configuration $[(0, 0, \uparrow)(0, 0, \downarrow)(0, 1, \uparrow)]$, and has the total spin $S_{tot} = 1/2$. This state is four-fold degenerate ($L_{tot} = \pm 1/2$, $S_{\zeta}^{tot} = \pm 1/2$).

Figure 3 shows the low-lying energy levels with the total angular momentum $L_{tot} = 0$. Shown are only the states which start from $E/\hbar\omega_0 \leq 7$ at $\lambda = 0$. The lowest-energy state has the total spin $S_{tot} = 3/2$ and four-fold degeneracy ($S_{\zeta}^{tot} = \pm 3/2, \pm 1/2$). In the limit $\lambda \rightarrow 0$ the state with the full spin polarization ($S_{tot} = 3/2, S_{\zeta}^{tot} = +3/2$) corresponds to the configuration

$$[(0, -1, \uparrow)(0, 0, \uparrow)(0, 1, \uparrow)]. \quad (25)$$

The state with a partial spin polarization ($S_{tot} = 3/2, S_{\zeta}^{tot} = +1/2$) corresponds in the limit $\lambda \rightarrow 0$ to the configuration

$$\frac{1}{\sqrt{3}}(\Psi_1 + \Psi_2 + \Psi_3), \quad (26)$$

where

$$\begin{aligned} \Psi_1 &= [(0, -1, \downarrow)(0, 0, \uparrow)(0, 1, \uparrow)], \\ \Psi_2 &= [(0, -1, \uparrow)(0, 0, \downarrow)(0, 1, \uparrow)], \\ \Psi_3 &= [(0, -1, \uparrow)(0, 0, \uparrow)(0, 1, \downarrow)]. \end{aligned} \quad (27)$$

The state with $S_{tot} = 3/2$ and $S_{\zeta}^{tot} = +1/2$ was not found in previous calculations.

I performed similar calculations for L_{tot} from 0 to 9 and for all total-spin states $S_{tot} = 3/2$ and $1/2$. Results for L_{tot} from 0 to 2 are shown in Figure 4. *Only the lowest-energy levels ($m = 1$) for each pair of numbers (L_{tot}, S_{tot}) are shown in the Figure* [this means that, say, a $(1, 1/2)$ -level with $m > 1$ (not shown in the Figure) may have the lower energy than the exhibited level $(2, 3/2)$ with $m = 1$]. One sees that the most important energy levels are $(1, 1/2)$ and $(0, 3/2)$: at small λ the former state is the ground state and the latter one is the first excited state; at larger λ ($\lambda \gtrsim 4$) the state $(0, 3/2)$ becomes the ground, and the state $(1, 1/2)$ – the first excited state. More clearly it is seen in Figure 5 where the difference between the energies of the states $(0, 3/2)$ and $(1, 1/2)$ is exhibited as a function of the interaction parameter. The transition $(1, 1/2) \leftrightarrow (0, 3/2)$ between the two states with different total spin quantum numbers occurs at $\lambda = \lambda_c = 4.343$. At large λ (more exactly, at $\lambda = 10$) the energy difference is $E_{(0,3/2)} - E_{(1,1/2)} \approx -0.0416\hbar\omega_0$. The total momentum of the system (the sum of the total orbital momentum and the total spin) does not change at the transition point.

In Table I exact results for the energies of the states $(1, 1/2)$ and $(0, 3/2)$ are compared with QMC results from Ref.³². One sees that the accuracy of the QMC results³² is in general very high, but the errors are not always small (see e.g. $\lambda = 10$) compared to the *difference* between the energies of the ground and excited states.

It should be emphasized that the transition $(L_{tot}, S_{tot}) = (1, 1/2) \rightarrow (0, 3/2)$ is *not* a transition to a *fully spin-polarized* state, as was asserted in some publications. The transition occurs to the state with $S_{tot} = 3/2$, where S_{tot} is the *total spin* quantum number, but not its projection S_{ζ}^{tot} . The energies of all four $(0, 3/2)$ -states with $S_{\zeta}^{tot} = \pm 3/2$ and $\pm 1/2$ are exactly the same, i.e. the state $(L_{tot}, S_{tot}) = (0, 3/2)$ is degenerate with respect to the projection of the total spin, as it obviously should be in the absence of magnetic field.

2. Approximations

The energy of the states $(1, 1/2)$ and $(0, 3/2)$ can be approximated, in the interval $0 \leq \lambda \leq 10$, by the formula

$$E = E_{GS}^{cl} + \epsilon_{cl} \left(AX + \sqrt{B^2 + C^2 X^2} - B \right), \quad (28)$$

where E_{GS}^{cl} is the classical ground state energy (22), $X = \hbar\omega_0/\epsilon_{cl}$, and the numbers A, B, C for the two considered states are

$$(A, B, C)_{(1,1/2)} = (3.11536, 2.93076, 0.917954), \quad (29)$$

$$(A, B, C)_{(0,3/2)} = (2.84171, 2.44529, 2.13633). \quad (30)$$

For the state $(1, 1/2)$ the difference between the exact energy and the approximation (28)–(29) is about 0.83% at $\lambda = 0$, does not exceed 0.22% at $0.05 \leq \lambda \leq 10$, and tends to zero with growing λ . For the state $(0, 3/2)$ the difference between the exact solution and the approximation is smaller than 0.44% in the whole range of λ . It should be noted however, that the *difference* between the energies of the two states $E_{(0,3/2)} - E_{(1,1/2)}$ is reproduced by the approximate formulas (28)–(30) with a substantially worse accuracy.

C. Heat capacity

Figure 6 exhibits the calculated low-temperature heat capacity C_λ as a function of T and λ . About 30 lowest-energy levels for each L_{tot} from 0 to 9, with corresponding degeneracies, were taken into account in this calculation. A pronounced peak related to the gap between the ground and the first excited state can be clearly seen in this Figure. The value of the peak temperature $T_p(\lambda)$ depends on λ as $|E_{(0,3/2)} - E_{(1,1/2)}|$ (compare to Figure 5), and disappears at the transition point $\lambda = \lambda_c$. The most dramatic variations of the heat capacity are the case in the range $kT \lesssim 0.1\hbar\omega_0$, which corresponds, at a typical confinement of GaAs quantum dots ($\hbar\omega_0 \sim 3$ meV), to a few-K temperature scale.

D. Electron density

Due to rotational symmetry of the Hamiltonian (1) the density of spin-up and spin-down polarized electrons in the quantum-mechanical states (L_{tot}, S_{tot}) does not depend on the angular coordinate θ , $n_\sigma^{(L_{tot}, S_{tot})}(r, \theta) = n_\sigma^{(L_{tot}, S_{tot})}(r)$, for $\sigma = \uparrow$ or \downarrow . Figures below show the density of electrons as a function of r only.

1. The state $(L_{tot}, S_{tot}) = (0, 3/2)$

The total density of electrons $n^{(0,3/2)}(r) = n_\uparrow^{(0,3/2)}(r) + n_\downarrow^{(0,3/2)}(r)$ in the state $(L_{tot}, S_{tot}) = (0, 3/2)$ at a few values of the interaction parameter λ is shown in Figure 7. The function $n^{(0,3/2)}(r)$ also determines the densities of spin-up and spin-down polarized electrons: in the state with the total spin projection $S_\zeta^{tot} = +3/2$ they are

$$n_\uparrow^{(0,3/2,+3/2)}(r) = n^{(0,3/2)}(r), \quad n_\downarrow^{(0,3/2,+3/2)}(r) = 0; \quad (31)$$

in the state $S_\zeta^{tot} = +1/2$

$$\begin{aligned} n_\uparrow^{(0,3/2,+1/2)}(r) &= \frac{2}{3}n^{(0,3/2)}(r), \\ n_\downarrow^{(0,3/2,+1/2)}(r) &= \frac{1}{3}n^{(0,3/2)}(r). \end{aligned} \quad (32)$$

Figure 7 shows that in the state $(0, 3/2)$ electrons are strongly correlated even at very small λ – they repel each other, and the maximum of the electron density lies at a finite distance from the origin even at $\lambda \ll 1$. At $\lambda \gtrsim 1$ the maxima of the electron density are very close to the classical radii (21), shown by triangles on the Figure. Recall that at $\lambda > \lambda_c = 4.343$ the state $(0, 3/2)$ is the ground state, and as seen from the Figure, at these λ 's the density of electrons qualitatively corresponds to the angle-averaged classical distribution of particles (a Wigner molecule).

2. The state $(L_{tot}, S_{tot}) = (1, 1/2)$

In the state $(1, 1/2)$ the spatial distribution of electrons is less trivial. Now we have two sorts of particles: two electrons are polarized up, and one electron is polarized down. They cannot be arranged in the highly symmetric structure of an equilateral triangle, as three equally polarized electrons. How they are distributed in space is seen from Figures 8, 9, and 10. Figure 8 exhibits the total electron density (spin-up plus spin-down). One sees that at small λ electrons behave as non- or weakly interacting particles, forming the structure with a maximum of the electron density at $r = 0$. Such a picture is the case up to $\lambda \simeq 2$, when a weak minimum of the density at $r = 0$ appears. At even larger λ the influence of electron-electron interaction becomes more important: the density of electrons qualitatively looks like in the state $(0, 3/2)$, with a minimum at $r = 0$ and maxima close to the classical radii (21).

Additional and even more interesting information about the spatial distribution of electrons can be extracted from Figures 9 and 10, which show separately the densities of spin-up and spin-down polarized electrons. At small λ the one spin-down electron occupies the center of the dot, while the two spin-up electrons rotate around the center with a maximum of the density at a finite distance from the origin. Such a situation is a peculiar quantum-mechanical feature: it is not encountered in the classical picture. The structure “one electron in the center, two electrons around” conserves up to $\lambda \simeq 2$: the density of the spin-up electrons has a clear maximum at a finite distance from the origin, while the oppositely polarized electron is still centered at $r = 0$. At even larger λ ($\gtrsim 4$), electron-electron interaction pushes the spin-down electron out from the center: the density maximum of the spin-down electron is shifted to a finite r . Due to that, electrons have a tendency to form a triangular structure similar to the classical one. For the state $(1, 1/2)$, however, such a structure would not have a proper symmetry, as electrons have different spin. As

a consequence, the system switches to a more symmetric $(0, 3/2)$ ground state.

3. At the transition point

Exactly at the transition point $\lambda = \lambda_c$ the density of electrons in the ground state changes very sharply, Figure 11. Electrons are pushed out from the center of the dot when the system passes from the state $(1, 1/2)$ to the state $(0, 3/2)$, with a 30% reduction of the density at the point $r = 0$.

The value

$$A = \frac{1}{N} \int dr \pi r^2 n_e(r) = \frac{\pi}{N} \langle \Psi_{GS} | \sum_i r_i^2 | \Psi_{GS} \rangle \quad (33)$$

[$n_e(r)$ is the total electron density, Ψ_{GS} is the ground-state wave function] can be treated as the “volume” of the dot. The curvature $K \propto \omega_0^2 \propto \lambda^{-4}$ of the confinement potential can be considered as a “pressure” acting on electrons of the dot from the confining potential. The diagram A versus λ^{-4} is thus qualitatively equivalent to the volume-pressure dependence for a macroscopic system. Figure 12 shows such a diagram for a three-electron quantum dot in the vicinity of the transition point. One sees that the “volume” discontinuously jumps down at $\lambda = \lambda_c$. When the pressure is small (λ is large, the strong Coulomb interaction regime), electrons form an equilateral-triangle structure. Increasing the pressure reduces the area of this triangle. Further increase of the curvature leads to a phase transition at the critical point $\lambda = \lambda_c$: the equilateral triangle is reconstructed to a more compact structure with one (spin-down) electron in the center and two (spin-up) electrons rotating around. This transition is accompanied by a jump of the “volume” of the dot, with a δ -like peculiarity in the compressibility.

As seen from the density pictures, the state $(0, 3/2)$ has evident Wigner-crystal properties, while the state $(1, 1/2)$ is of a liquid type. The transition at $\lambda = \lambda_c$ is thus a precursor of the liquid-solid transitions in macroscopic 2D systems⁴⁶. In a three-electron quantum dot it happens however at a substantially smaller relative strength of electron-electron interaction than in the bulk 2DES.

E. Pair-correlation functions

The pair-correlation function $P_{\sigma\sigma'}(\mathbf{r}, \mathbf{r}')$ determines the probability to find electron with the spin σ at the point \mathbf{r} , under the condition that another electron with the spin σ' is fixed at the point \mathbf{r}' . Figures below show $\hat{P}_{\sigma\sigma'}(\mathbf{r}, \mathbf{r}')$ as a function of \mathbf{r}/l_0 for both orientations of the spin σ (\uparrow or \downarrow). The second electron, also with the spin $\sigma' = \uparrow$ or \downarrow , is assumed to be fixed at the classical distance (21) from the origin, $\mathbf{r}' = (0, -R_{cl})$ (the *second* subscript corresponds to the spin of a fixed electron).

1. The state $(L_{tot}, S_{tot}) = (0, 3/2)$

Figure 13 exhibits the pair-correlation function $P_{\uparrow\uparrow}(\mathbf{r}, \mathbf{r}')$ in the state $(L_{tot}, S_{tot}, S_{\zeta}^{tot}) = (0, 3/2, +3/2)$. The interaction parameter λ assumes the values 0.1, 2, 4, and 8, from up to down. At small λ electron-electron interaction is weak, and the pair-correlation function has a form of a single peak centered opposite to the fixed electron. With growing λ this peak is splitted onto two ones, and this splitting becomes very pronounced at strong Coulomb interaction ($\lambda \gtrsim 4$). In this regime the pair-correlation function evidently corresponds to the classical picture of a triangular electron configuration.

In the case of $S_{\zeta}^{tot} = +3/2$, three other pair-correlation functions are obviously zero, $P_{\uparrow\downarrow} = P_{\downarrow\uparrow} = P_{\downarrow\downarrow} = 0$. In the state $(L_{tot}, S_{tot}) = (0, 3/2)$ with $S_{\zeta}^{tot} = +1/2$, all the pair-correlation functions are proportional to that shown in Figure 13,

$$P_{\uparrow\uparrow, \uparrow\downarrow, \downarrow\uparrow}^{(0, 3/2, +1/2)} = \frac{1}{3} P_{\uparrow\uparrow}^{(0, 3/2, +3/2)}, \quad (34)$$

and $P_{\downarrow\downarrow}^{(0, 3/2, +1/2)} = 0$.

2. The state $(L_{tot}, S_{tot}) = (1, 1/2)$

In the state $(L_{tot}, S_{tot}, S_{\zeta}^{tot}) = (1, 1/2, +1/2)$ the function $P_{\uparrow\uparrow}$, Figure 14, is qualitatively similar to that of the $(0, 3/2)$ state, but the splitting of the maximum of the pair correlation function becomes visible at substantially larger λ . At $\lambda = 2$ it is not yet seen at all, and at $\lambda = 4$ is still rather weak. This supports the above interpretation of this state as the state of a liquid type at $\lambda \lesssim 4$. In the regime of very strong Coulomb interaction ($\lambda = 8$) the function $P_{\uparrow\uparrow}^{(1, 1/2)}$ exhibits a triangular structure similar to the state $(0, 3/2)$.

The functions $P_{\uparrow\downarrow}$ (Figure 15) and $P_{\downarrow\downarrow}$ (Figure 16), describing correlations between electrons with opposite spins ($\sigma \neq \sigma'$), have a specific feature at small λ , showing a gaussian-type form, centered at $r = 0$. This picture agrees with the form of the density of spin-up and spin-down polarized electrons which was discussed in Section III D, Figures 9 and 10. With the growing λ these gaussian-type peaks are splitted, like in two previous Figures. It is interesting to notice that this splitting is the case for both the function $P_{\uparrow\downarrow}$ (one down-electron is fixed and *two* up-electrons are splitted), and the function $P_{\downarrow\downarrow}$ (one up-electron is fixed and *the only one* down-electron is splitted). This gives an additional physical argument in favour of the transition $(1, 1/2) \rightarrow (0, 3/2)$: due to the wave nature of electrons each of the two spin subsystems should assume the triangular structure in the regime of strong Coulomb interaction, but it is easier to do if all three electrons are in the same spin state.

The fourth function $P_{\downarrow\downarrow}$ is evidently zero in the state $(1, 1/2)$.

IV. DISCUSSION AND SUMMARY

Properties of the dot are governed by the only dimensionless parameter λ , which characterizes the relative strength of Coulomb and quantum effects. At small λ the Coulomb interaction is not essential and electrons occupy the lowest possible energy states which evidently leads to the $(1, 1/2)$ ground state. At large λ (quasi-classical situation) point particles would arrange themselves in an equilateral triangle. For quantum particles, however, the question arises what are the spin states of three electrons occupying the corners of the triangle. From the symmetry considerations it seems to be obvious that all spins should be the same, which leads to a conclusion that at large λ the total spin of the dot should be $3/2$. Hence, anywhere at finite λ a transition $(1, 1/2) \leftrightarrow (0, 3/2)$ should be the case, and calculations show that in a purely parabolic quantum dot it happens at $\lambda = \lambda_c = 4.343$. As shown in Section III, this transition is accompanied by a dramatic change of properties of the dot, and can be treated as a liquid-solid transition.

The transition $(1, 1/2) \rightarrow (0, 3/2)$ should be observable in many experiments. It should manifest itself in any thermodynamic quantity. The difference in the ground-state total spin S_{tot} should be also seen in the Zeeman and spin splitting of levels in magnetic field, both parallel and perpendicular to the plane of 2DES. The structure of levels could be also studied by Raman spectroscopy.

The method of the paper can be used for studying systems with more particles and/or in a non-parabolic confinement potential⁵³. It can also be used for investigating other properties of the system, for instance, the influence of impurities, or response of the dot to external fields. It is seen already now, for instance, that an asymmetrically located impurity will qualitatively differently affect the ground state of the dot at $\lambda < \lambda_c$ and at $\lambda > \lambda_c$. In the former case the ground state $(1, 1/2)$ is degenerate with respect to L_{tot} , and the presence of an impurity will result in a *splitting* of the ground state level. In the latter case the ground state $(0, 3/2)$ is non-degenerate with respect to L_{tot} , and the impurity will lead to a *shift* of the ground state energy. This may lead to interesting consequences in the physics of the liquid-solid transition in a quantum dot with disorder.

To summarize, I have performed a complete theoretical study of a system of three Coulomb-interacting electrons in a parabolic quantum dot, and investigated in detail physical properties and the origin of the Fermi liquid – Wigner solid transition in the ground state of the dot.

ACKNOWLEDGMENTS

The work was supported by the Sonderforschungsbereich SFB 484, University of Augsburg. I thank Klaus Ziegler, Ulrich Eckern and Vladimir Sablikov for useful discussions.

- ¹ L. Jacak, P. Hawrylak, and A. Wojs, *Quantum Dots* (Springer, Berlin, 1997).
- ² R. C. Ashoori, *Nature* **379**, 413 (1996).
- ³ L. P. Kouvenhoven *et al.*, in *Mesoscopic Electron Transport*, edited by L. L. Sohn, L. P. Kouvenhoven, and G. Schön (Kluwer Academic Publisher, Dordrecht, 1997), Vol. 345.
- ⁴ D. Heitmann and J. P. Kotthaus, *Physics Today* **46**, 56 (June 1993).
- ⁵ C. Schüller, in *Festkörperprobleme/Adv. in Solid State Physics*, edited by B. Kramer (Vieweg, Braunschweig, 1998), Vol. 38, p. 167.
- ⁶ M. Taut, *Phys. Rev. A* **48**, 3561 (1993).
- ⁷ M. Taut, *J. Phys. A.: Math. Gen.* **27**, 1045 (1994).
- ⁸ A. Turbinger, *Phys. Rev. A* **50**, 5335 (1994).
- ⁹ M. Dineykhani and R. G. Nazmitdinov, *Phys. Rev. B* **55**, 13707 (1997).
- ¹⁰ M. Taut, *J. Phys. Condens. Matter* **12**, 3689 (2000).
- ¹¹ P. A. Maksym and T. Chakraborty, *Phys. Rev. Lett.* **65**, 108 (1990).
- ¹² U. Merkt, J. Huser, and M. Wagner, *Phys. Rev. B* **43**, 7320 (1991).
- ¹³ D. Pfannkuche and R. R. Gerhardts, *Phys. Rev. B* **44**, 13132 (1991).
- ¹⁴ M. Wagner, U. Merkt, and A. V. Chaplik, *Phys. Rev. B* **45**, 1951 (1992).
- ¹⁵ P. Hawrylak and D. Pfannkuche, *Phys. Rev. Lett.* **70**, 485 (1993).
- ¹⁶ A. H. MacDonald and M. D. Johnson, *Phys. Rev. Lett.* **70**, 3107 (1993).
- ¹⁷ S.-R. E. Yang, A. H. MacDonald, and M. D. Johnson, *Phys. Rev. Lett.* **71**, 3194 (1993).
- ¹⁸ D. Pfannkuche, V. Gudmundsson, and P. A. Maksym, *Phys. Rev. B* **47**, 2244 (1993).
- ¹⁹ J. J. Palacios *et al.*, *Phys. Rev. B* **50**, 5760 (1994).
- ²⁰ F. M. Peeters and V. A. Schweigert, *Phys. Rev. B* **53**, 1468 (1996).
- ²¹ T. Ezaki, N. Mori, and C. Hamaguchi, *Phys. Rev. B* **56**, 6428 (1997).
- ²² M. Eto, *Jpn. J. Appl. Phys.* **36**, 3924 (1997).
- ²³ C. E. Creffield, W. Häusler, J. H. Jefferson, and S. Sarkar, *Phys. Rev. B* **59**, 10719 (1999).
- ²⁴ S. M. Reimann, M. Koskinen, and M. Manninen, *Phys. Rev. B* **62**, 8108 (2000).
- ²⁵ C. Yannouleas and U. Landman, *Phys. Rev. Lett.* **85**, 1726 (2000).
- ²⁶ P. A. Maksym, *Phys. Rev. B* **53**, 10871 (1996).
- ²⁷ F. Bolton, *Phys. Rev. B* **54**, 4780 (1996).
- ²⁸ A. Harju, V. A. Sverdlov, and R. M. Nieminen, *Europhys. Lett.* **41**, 407 (1998).
- ²⁹ A. Harju, V. A. Sverdlov, R. M. Nieminen, and V. Halonen, *Phys. Rev. B* **59**, 5622 (1999).
- ³⁰ A. Harju, S. Siljamäki, and R. M. Nieminen, *Phys. Rev. B* **60**, 1807 (1999).
- ³¹ R. Egger, W. Häusler, C. H. Mak, and H. Grabert, *Phys. Rev. Lett.* **82**, 3320 (1999).

- ³² R. Egger, W. Häusler, C. H. Mak, and H. Grabert, Phys. Rev. Lett. **83**, 462(E) (1999).
- ³³ F. Pederiva, C. J. Umrigar, and E. Lipparini, Phys. Rev. B **62**, 8120 (2000).
- ³⁴ A. V. Filinov, M. Bonitz, and Y. E. Lozovik, Phys. Rev. Lett. **86**, 3851 (2001).
- ³⁵ K. Hirose and N. S. Wingreen, Phys. Rev. B **59**, 4604 (1999).
- ³⁶ O. Steffens, U. Rössler, and M. Suhrke, Europhys. Lett. **42**, 529 (1998).
- ³⁷ O. Steffens, U. Rössler, and M. Suhrke, Europhys. Lett. **44**, 222 (1998).
- ³⁸ O. Steffens, M. Suhrke, and U. Rössler, Physica B **256-258**, 147 (1998).
- ³⁹ A. Wensauer, O. Steffens, M. Suhrke, and U. Rössler, Phys. Rev. B **62**, 2605 (2000).
- ⁴⁰ P. A. Maksym, Europhys. Lett. **31**, 405 (1995).
- ⁴¹ W. Y. Ruan, Y. Y. Liu, C. G. Bao, and Z. Q. Zhang, Phys. Rev. B **51**, 7942 (1995).
- ⁴² W. Häusler, Z. Phys. B **99**, 551 (1996).
- ⁴³ C. Yannouleas and U. Landman, Phys. Rev. Lett. **82**, 5325 (1999).
- ⁴⁴ W. Häusler, Europhys. Lett. **49**, 231 (2000).
- ⁴⁵ B. Reusch, W. Häusler, and H. Grabert, Phys. Rev. B **63**, 113313 (2001).
- ⁴⁶ B. Tanatar and D. M. Ceperley, Phys. Rev. B **39**, 5005 (1989).
- ⁴⁷ S. T. Chui and B. Tanatar, Phys. Rev. Lett. **74**, 458 (1995).
- ⁴⁸ E. Abrahams, S. V. Kravchenko, and M. P. Sarachik, Rev. Mod. Phys. **73**, 251 (2001).
- ⁴⁹ V. Fock, Z. Phys. **47**, 446 (1928).
- ⁵⁰ C. G. Darwin, Cambridge Phil. Soc. **27**, 86 (1931).
- ⁵¹ F. Bolton and U. Rössler, Superlatt. Microstruct. **13**, 139 (1993).
- ⁵² V. M. Bedanov and F. M. Peeters, Phys. Rev. B **49**, 2667 (1994).
- ⁵³ S. A. Mikhailov, preprint *cond-mat/0106369* (unpublished).

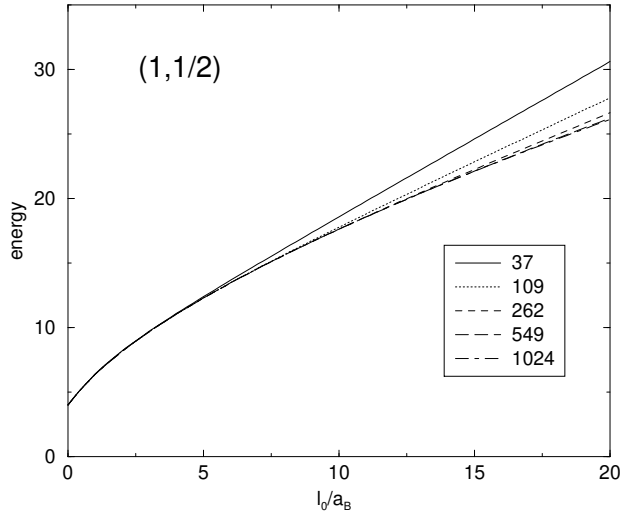


FIG. 1. Convergence of the energy of the lowest state with $(L_{tot}, S_{tot}) = (1, 1/2)$. The energy unit is $\hbar\omega_0$. The curves are labeled by the number of many-body states involved in the expansion (9).

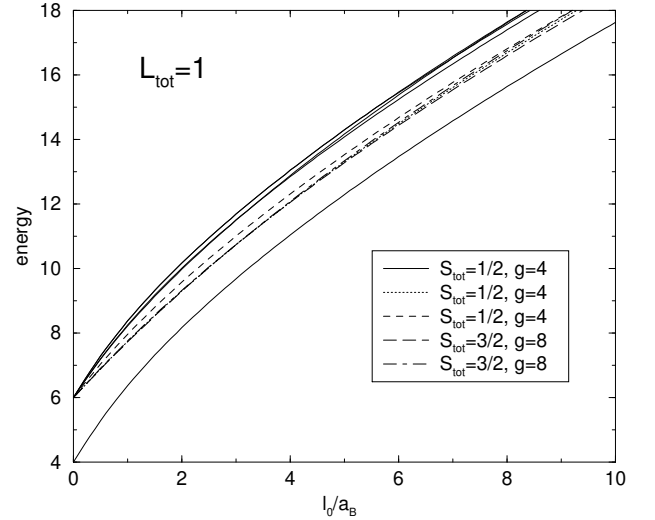


FIG. 2. Low-lying energy levels with the total angular momentum $L_{tot} = 1$ in a 3-electron quantum dot. The energy unit is $\hbar\omega_0$. The five lowest levels are labeled by their total spin S_{tot} and the degeneracy g .

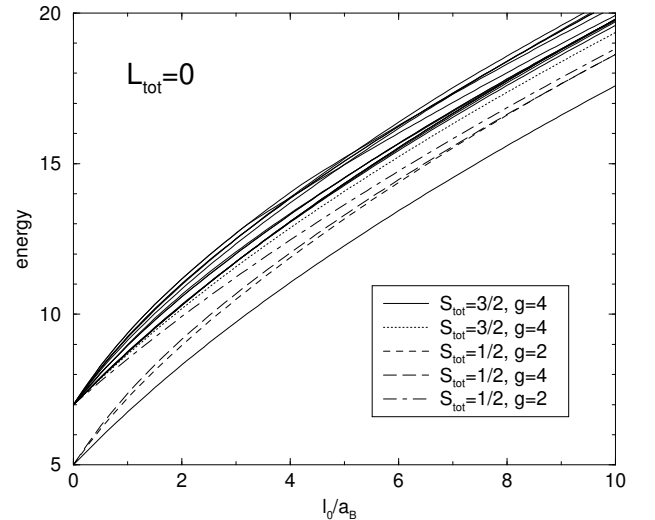


FIG. 3. Low-lying energy levels with the total angular momentum $L_{tot} = 0$ in a 3-electron quantum dot. The energy unit is $\hbar\omega_0$. The five lowest levels are labeled by their total spin S_{tot} and the degeneracy g .

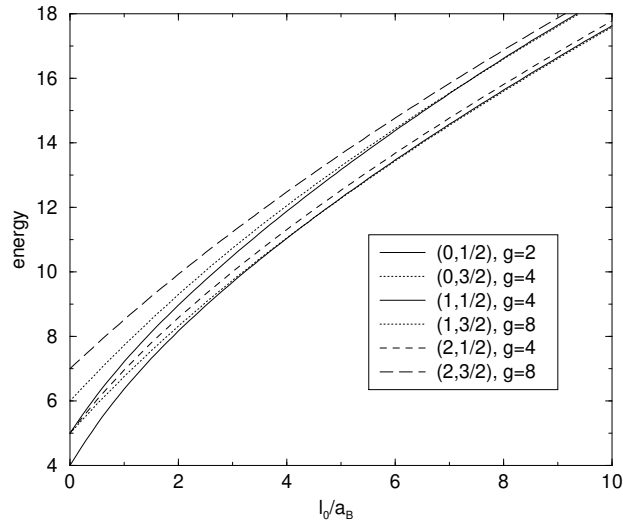


FIG. 4. Low-lying energy levels in a 3-electron quantum dot, for the total angular momentum L_{tot} from 0 to 2 and for all total spin states. Only the one lowest-energy level is shown for each pair of quantum numbers (L_{tot}, S_{tot}) . The energy unit is $\hbar\omega_0$. The levels are labeled by the pair of quantum numbers (L_{tot}, S_{tot}) and the degeneracy g .

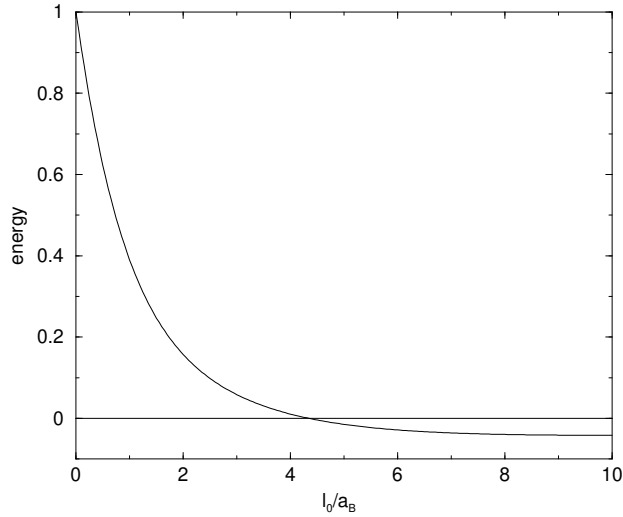


FIG. 5. Energy difference between the lowest states $E_{(0,3/2)} - E_{(1,1/2)}$ in a 3-electron quantum dot as a function of the interaction parameter $\lambda = l_0/a_B$. The energy unit is $\hbar\omega_0$. The transition occurs at $\lambda = \lambda_c \approx 4.343$. $E_{(0,3/2)} - E_{(1,1/2)} \approx -0.0416\hbar\omega_0$ at $\lambda = 10$.

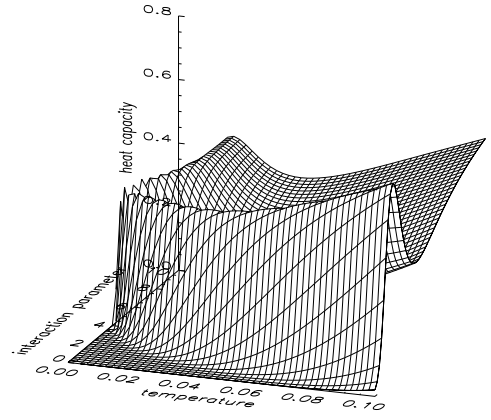


FIG. 6. Heat capacity of a 3-electron parabolic quantum dot, as a function of the temperature $kT/\hbar\omega_0$ and the interaction parameter l_0/a_B .

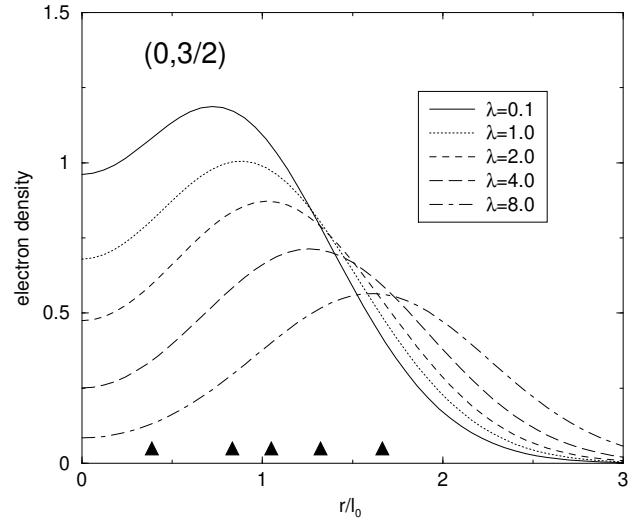


FIG. 7. Total electron density (spin-up plus spin-down) in the state $(L_{tot}, S_{tot}) = (0, 3/2)$ at different λ . Triangles show the positions of the classical radius (21) at corresponding values of λ .

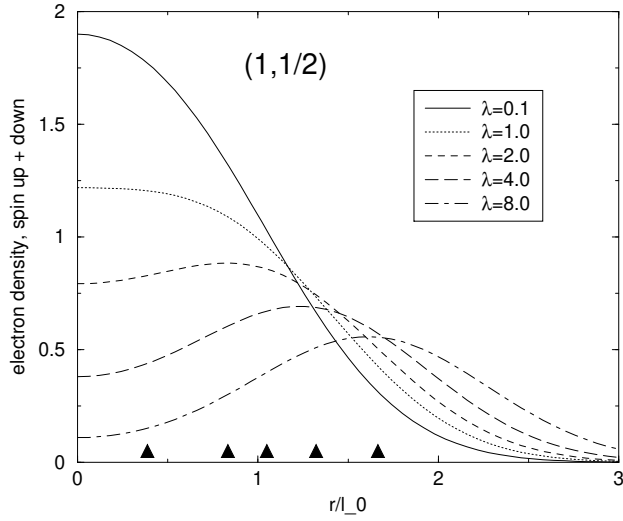


FIG. 8. Total electron density (spin-up plus spin-down) in the state $(1,1/2)$ at different λ . Triangles show the positions of the classical radius (21) at corresponding values of λ .

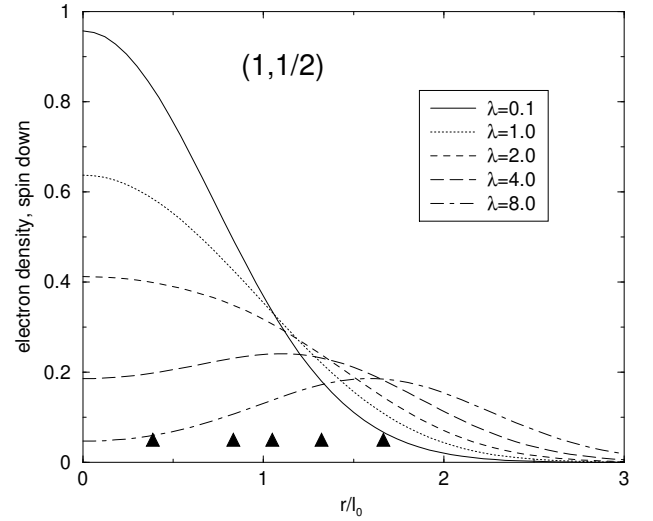


FIG. 10. Density of spin-down polarized electrons in the state $(1,1/2)$ at different λ . Triangles show the positions of the classical radius (21) at corresponding values of λ .

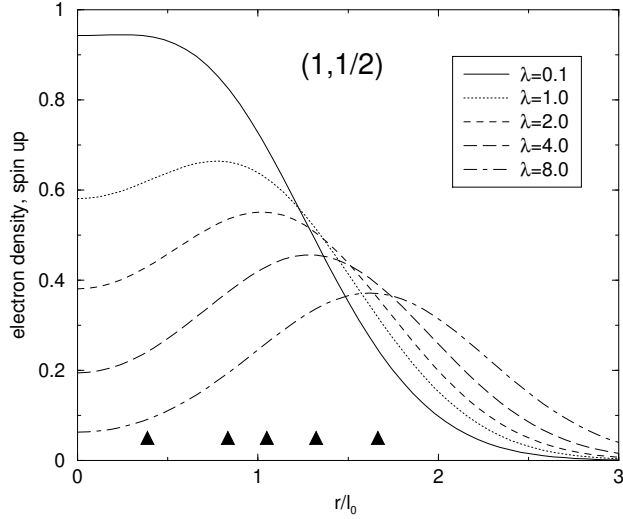


FIG. 9. Density of spin-up polarized electrons in the state $(1,1/2)$ at different λ . Triangles show the positions of the classical radius (21) at corresponding values of λ .

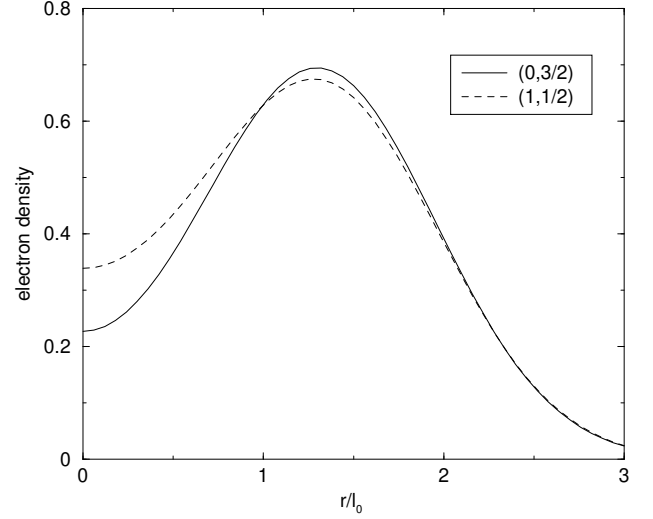


FIG. 11. Electron density in the states $(1,1/2)$ (the ground state at $\lambda < \lambda_c$) and $(0,3/2)$ (the ground state at $\lambda > \lambda_c$) at the transition point $\lambda = \lambda_c = 4.343$.

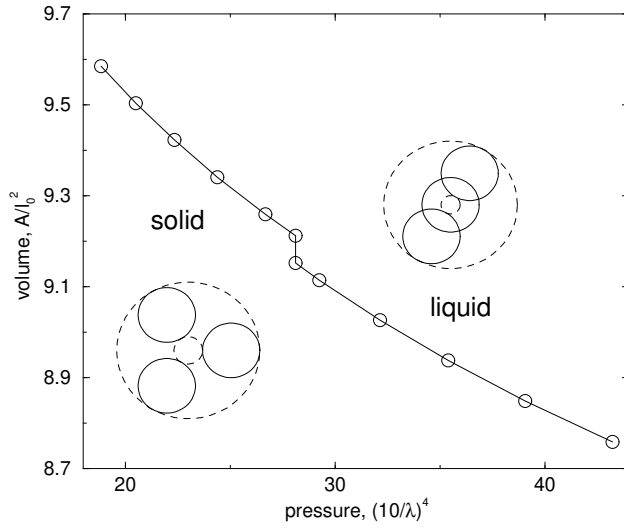


FIG. 12. A “volume”-“pressure” diagram, A/l_0^2 versus $(10/\lambda)^4$, for a quantum dot lithium in the vicinity of the transition point $\lambda = \lambda_c = 4.343$. Insets schematically show the distribution of electrons in the dot in the solid and liquid phases.

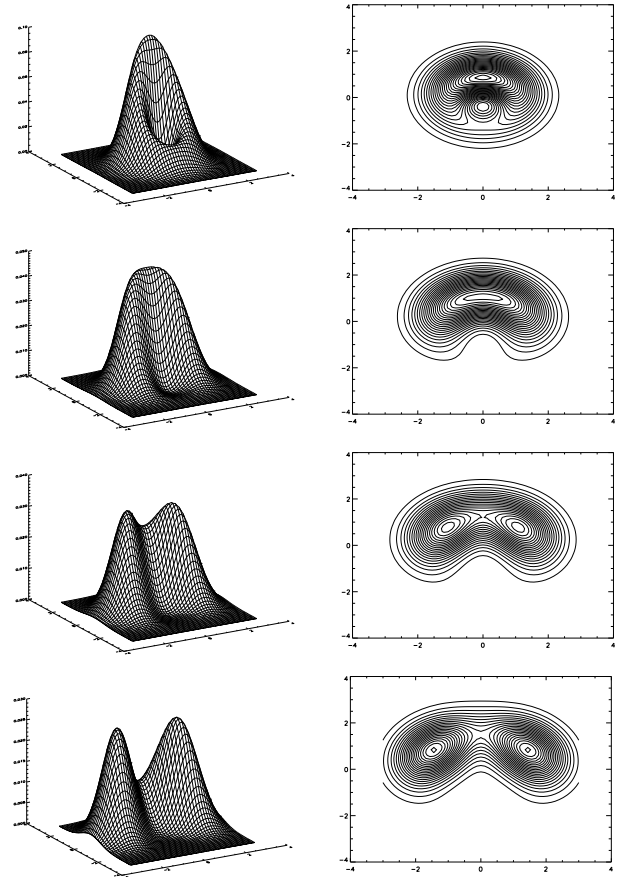


FIG. 14. Pair-correlation function $P_{\uparrow\uparrow}$ of the state with $L_{tot} = 1$, $S_{tot} = 1/2$, $S_{\zeta}^{tot} = +1/2$, at $\lambda = 0.1, 2, 4,$ and 8 , from up to down ($|\mathbf{r}'|/l_0 = R_{cl}/l_0 = 0.38, 1.04, 1.32,$ and 1.66 , respectively).

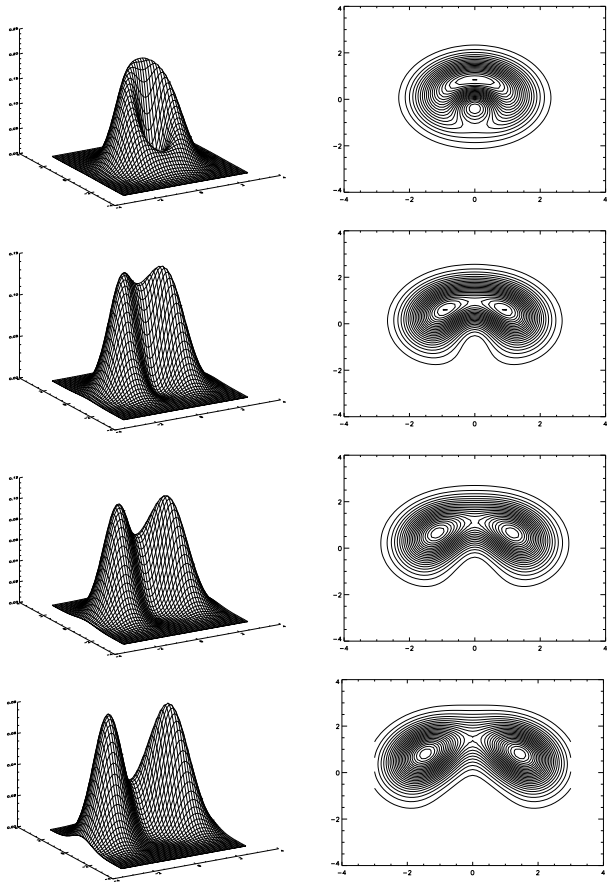


FIG. 13. Pair-correlation function $P_{\uparrow\uparrow}$ of the state with $L_{tot} = 0$, $S_{tot} = 3/2$, $S_{\zeta}^{tot} = +3/2$, at $\lambda = 0.1, 2.0, 4.0,$ and 8.0 , from up to down ($|\mathbf{r}'|/l_0 = R_{cl}/l_0 = 0.38, 1.04, 1.32,$ and 1.66 , respectively).

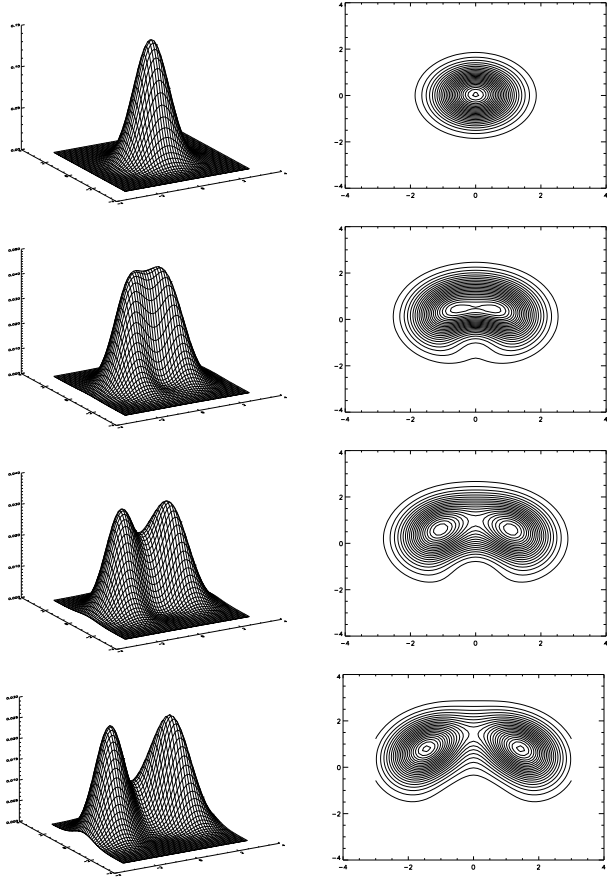


FIG. 15. Pair-correlation function $P_{1\uparrow}$ of the state with $L_{tot} = 1$, $S_{tot} = 1/2$, $S_{\zeta}^{tot} = +1/2$, at $\lambda = 0.1, 2, 4$, and 8 , from up to down ($|\mathbf{r}'|/l_0 = R_{cl}/l_0 = 0.38, 1.04, 1.32$, and 1.66 , respectively).

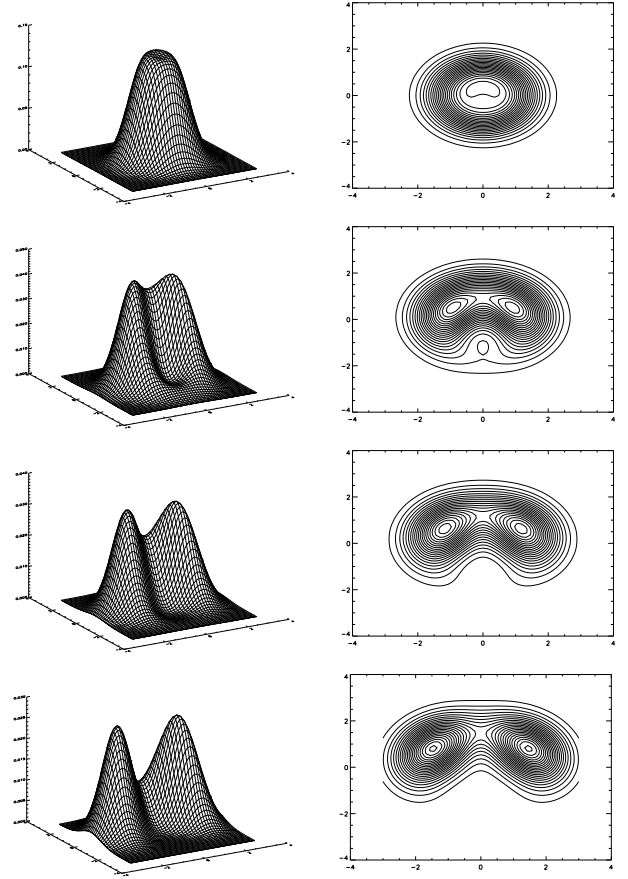


FIG. 16. Pair-correlation function $P_{1\downarrow}$ of the state with $L_{tot} = 1$, $S_{tot} = 1/2$, $S_{\zeta}^{tot} = +1/2$, at $\lambda = 0.1, 2, 4$, and 8 , from up to down ($|\mathbf{r}'|/l_0 = R_{cl}/l_0 = 0.38, 1.04, 1.32$, and 1.66 , respectively).

TABLE I. Energies of the states $(1,1/2)$ and $(0,3/2)$ calculated in this work (exact diagonalization) and in Ref.³² (QMC, multilevel blocking algorithm).

λ	$S_{tot} = 3/2$	$S_{tot} = 3/2^a$	$S_{tot} = 1/2$	$S_{tot} = 1/2^a$
2	8.3221	8.37(1)	8.1651	8.16(3)
4	11.0527	11.05(1)	11.0422	11.05(2)
6	13.4373	13.43(1)	13.4658	no data
8	15.5938	15.59(1)	15.6334	no data
10	17.5863	17.60(1)	17.6279	no data

^aRef.³²